

## Synthesis and DFT Study of the Complexation of Schiff Base Derived Curcumin and L-Tyrosine with Al(III), Ag(I), and Pb(II) Metal Ions

Ali Mahmood Ali<sup>1</sup>, Tagreed Hashim Al-Noor<sup>1</sup>, Eid Abdalrazaq<sup>2\*</sup>, and Abdel Aziz Qasem Jbarah<sup>2</sup>

<sup>1</sup>Department of Chemistry, Ibn Al-Haithem College of Education for Pure Science, Baghdad University, Baghdad, Iraq

<sup>2</sup>Department of Chemistry, College of Science, Al-Hussein Bin Talal University, Ma'an, Jordan

\* Corresponding author:

tel: +962-796862267

email: eidalzooby@yahoo.com

Received: December 13, 2020

Accepted: February 22, 2021

DOI: 10.22146/ijc.62188

**Abstract:** The multi-dentate Schiff base ligand ( $H_2L$ ), where  $H_2L=2,2'-(((1,3,5,6)-1-(3-(11-oxidaneryl)-15-methyl)-4-hydroxyphenyl)-7-(4-hydroxy-3-methoxyphenyl)hepta-1,6-diene-3,5-diylidene)bis(azanelylylidene))bis(3-(4-hydroxyphenyl)propanoic acid)$ , has been prepared from curcumin and L-Tyrosine amino acid. The synthesized Schiff base ligand ( $H_2L$ ) and the second ligand 1,10-phenanthroline (phen) are used to prepare the new complexes  $[Al(L)(phen)]Cl$ ,  $K[Ag(L)(phen)]$  and  $[Pb(L)(phen)]$ . The synthesized compounds are characterized by magnetic susceptibility measurements, micro elemental analysis (C.H.N), mass spectrometry, molar conductance, FT-infrared, UV-visible, atomic absorption (AA),  $^{13}C$ -NMR, and  $^1H$ -NMR spectral studies. The characterization of the synthesized complexes shows that the environment surrounding the central metal ion in the complexes adopted a distorted octahedral configuration. Moreover, the conductivity measurements show a non-electrolytic character for the  $[Pb(L)(phen)]$  complex and an electrolytic character for the  $[Al(L)(phen)]Cl$  and  $K[Ag(L)(phen)]$  complexes. The experimental infrared data are supported by density functional theory (DFT) calculations using the B3LYP level of theory and LANL2DZ basis set. The vibrational frequencies of the molecules are computed using the optimized geometry obtained from the DFT calculations. The calculated vibrational frequencies have been compared with obtained experimental values.  $^1H$  and  $^{13}C$ -NMR chemical shifts were computed for the  $H_2L$  ligand using the DFT/GIAO method. Additionally, the molecular electronic structures of the complexes have been investigated by DFT calculations.

**Keywords:** curcumin; L-tyrosine; silver; aluminium; lead; Schiff base

### ■ INTRODUCTION

Schiff base derived from curcumin has much attention due to its various medicinal properties against expanding and dangerous diseases, such as different types of cancer and diabetes. Curcumin has various biological activities includes antioxidant, anti-inflammatory, antiviral, antibacterial, and many more studies [1-2]. The curcumin Schiff base was coordinated to the metal ion due to their catalytic power and antioxidant activity of these complexes [3].

In drug design, targeting is an important phenomenon because toxicity is often encountered only if the drugs are not delivered to the specific tissues, cells, and receptors where they are required. If the active species of

drugs contain metal complexes, then the complexes can spontaneously undergo biological reactions such as ligand substitution and redox reactions. Thus, enumerating the mechanism of the active species on biological reactions is expected to yield valuable information about using the metal complexes as drugs [4].

During the last few decades, metal carboxylates have been the subject of extensive investigations because of their remarkable structural diversity and significant biological activity, for example, pesticidal, bactericidal, and antitumor agents [5]. The antimicrobial activities of lead compounds of Schiff base have been compared with the corresponding free Schiff bases and standard drugs

[6]. Silver-containing compounds are attractive because, in the range of the applicable concentrations, silver ions do not exhibit toxicity and carcinogenic activities. There is an increased interest in the potential use of silver (I) as a therapeutic agent for different antimicrobial applications [7].

Another attractive property of Schiff bases is their use as an effective corrosion inhibitor. They have been studied extensively as a class of ligands and are known to coordinate with metal ions through the azomethine nitrogen atom. The ligation nature of Schiff base shows a great potentiometric sensor as they have shown excellent selectivity, sensitivity, and stability for specific metal ions such as Ag(I), Al(III), Co(II), Cu(II), Gd(III), Hg(II), Ni(II), Pb(II), Y(III), and Zn(II), Fe(III), Cd(II). The bonding of Schiff base in their complexes is due to the donor nature of neutral N of azomethine linkage [8].

This research focused on the production and identification of Schiff bases derived from curcumin and L-Tyrosine amino acid and treatment with some metallic and non-metallic elements. Density functional theory (DFT) calculations, including geometry optimization, vibrational frequency analysis, and electronic structures, were reported for the synthesized molecules using the B3LYP level of theory and LANL2DZ basis set.

## ■ EXPERIMENTAL SECTION

### Materials

Aluminum chloride ( $\text{AlCl}_3$ , 99% Sigma-Aldrich, Germany), silver nitrate ( $\text{AgNO}_3$ ,  $\geq 99.0\%$ , Sigma-Aldrich, Germany), lead nitrate ( $\text{Pb}(\text{NO}_3)_2$ ,  $\geq 99.95\%$  Sigma-Aldrich, Germany), curcumin ( $\geq 98.0\%$  Sigma-Aldrich, Germany), L-Tyrosine ( $\geq 98\%$  Sigma-Aldrich, Germany), methanol ( $\geq 99.8\%$  Sigma-Aldrich, Germany) and dimethyl sulfoxide (DMSO,  $\geq 99.7\%$  Sigma-Aldrich, Germany) were used as supplied.

### Instrumentation

Melting points (M.P) were recorded by MPA160 – Digi Melt melting point apparatus. Elemental analyses (C, H, N) of ligand were performed by Eager300 for EA1112 Thermal Finnegan C.H.N.S 2400 elemental analyzer. The (AAS) analysis in complexes was recorded by using a fair

agreement method by used the device from type Shimadzu (A.A 620) atomic absorption spectrophotometer. The molar conductivity measurements of the complexes with  $10^{-3} \text{ mol L}^{-1}$  in dimethyl sulfoxide (DMSO) were performed by using a device digital conductivity series Ino.Lab.720. Magnetic measurements of the complexes were measured by using Balance Johnson Matthey. The mass spectrum of ligand was determined by using Ion source: Electron Impact (EI) 70eV mass spectra register on manufacturer company: Agilent Technology 1. MS Model: 5973 spectrometers. Ultraviolet-visible spectra were obtained by using DMSO as a solvent and a concentration of  $10^{-3} \text{ mol L}^{-1}$  for the ligand and complexes. Ultraviolet-visible spectra were carried by double-beam UV-visible spectrophotometry type U.V 160A (Shimadzu) at the range between 200 and 1100 nm with a 1 cm quartz cell. The Fourier-transform infrared spectra were recorded using KBr pellets on Shimadzu FT-IR 8400S spectrophotometry. The Fourier-transform infrared spectra were recorded at the range of 400 to 4000  $\text{cm}^{-1}$ .  $^1\text{H}$  and  $^{13}\text{C}$ -NMR spectra were obtained from (DMSO- $d_6$  Solution using an Inova 500 MHz.

### Procedure

#### Preparation of the ligand

The ligand (Schiff base) was prepared by condensation of L-Tyrosine (0.362 g, 2 mmol) dissolved in 25 mL of hot water-ethanol mixture (1:1, ratio) solution and Curcumin (0.368 g, 1 mmol) dissolved in 25 mL of hot ethanol. The mixture was refluxed for about 10 h with the TLC technique observed until obtained a yellow-brown precipitate. It was filtered and purified by repeated washing with water-ethanol, as recrystallized from hot ethanol. The preparation of the Schiff base ligand  $\text{H}_2\text{L}$  is summarized in Scheme 1. The yield of the prepared Schiff base ligand,  $\text{H}_2\text{L}$ , was 81% (solid, Color: pale brown, m.p. 150–152 °C). FTIR (KBr,  $\text{cm}^{-1}$ ): 3508 ( $\nu(\text{O}-\text{H})$ ,  $-\text{COOH}$ ), 3400 ( $\nu(\text{O}-\text{H})$ , phenolic), 1629 ( $\nu(\text{C}=\text{N})$ ), 1595 ( $\nu_{\text{as}}(\text{COO})$ ,  $-\text{COOH}$ ), 1425 ( $\nu_{\text{s}}(\text{COO})$ ,  $-\text{COOH}$ ), 1244 ( $\nu(\text{C}-\text{O})$ , phenolic). UV-Vis spectroscopy ( $10^{-3} \text{ mol L}^{-1}$  concentration in DMSO,  $\lambda_{\text{max}}$  nm): 272, 433.  $^1\text{H}$ -NMR (500 MHz, DMSO-

d6):  $\delta$  9.66 (bs, 2H, OH), 7.54 (d, 4H, C<sub>6</sub>H<sub>4</sub>), 7.31 (d, 4H, C<sub>6</sub>H<sub>4</sub>), 7.15 (s, 2H, C=CH), 6.83–6.66 (m, 6H, C<sub>6</sub>H<sub>3</sub>), 6.06 (s, 2H, C=CH), 3.83 (s, 6H, OCH<sub>3</sub>), 3.74–3.36 (m, 8H, CH, CH<sub>2</sub>). <sup>13</sup>C-NMR (500 MHz, DMSO-d<sub>6</sub>):  $\delta$  183.2, 166.4, 149.4, 148.0, 147.0, 140.7, 140.4, 130.3, 126.3, 123.1, 121.1, 120.8, 119.6, 119.5, 115.9, 115.7, 111.3, 111.3, 100.8, 55.7. Anal. Calcd. for C<sub>39</sub>H<sub>38</sub>N<sub>2</sub>O<sub>10</sub> (694.25 g/mol): C, 67.43; H, 5.51; N, 4.03; O, 23.03%. Found: C, 66.41; H, 5.39; N, 4.09%.

### Preparation of the [Pb(L)(phen)] complex

1.0 mmol of lead(II) nitrate is dissolved in 10 mL of absolute ethanol to obtain metal ion (Pb<sup>2+</sup>) solution. A ligand solution is obtained by dissolving 1.0 mmol of Schiff base ligand, 2.0 mmol of potassium hydroxide, and 1.0 mmol of 1,10-phenanthroline in 15 mL of absolute ethanol. The ligand solution is gradually added to the metal ion (Pb<sup>2+</sup>) solution with constant stirring for 30 min to obtain the precipitate. The precipitate is filtrated and washed several times in a mixture of solvent (ethanol: distilled water, 50%). The precipitate is recrystallized from the hot ethanol. The preparation of the [Pb(L)(phen)] complex is summarized in Scheme 2. The yield of the [Pb(L)(phen)] complex, was 89% (solid, Color: brown, m.p. 156–158 °C). FTIR (KBr, cm<sup>-1</sup>): 3435 ( $\nu$ (O–H), phenolic), 1620 ( $\nu$ (C=N)), 1581 ( $\nu_{as}$ (COO), –COOH), 1384 ( $\nu_s$ (COO), –COOH), 1246 ( $\nu$ (C–O), phenolic), 576 ( $\nu$ (Pb–O)), 464 ( $\nu$ (Pb–N)). UV-Vis spectroscopy (10<sup>-3</sup> mol L<sup>-1</sup> concentration in DMSO,  $\lambda_{max}$  nm): 271, 435, 735. Metal percent in [Pb(L)(phen)] complex, calculated: 19.18%. Found: 18.01%. Molar conductivity (10<sup>-3</sup> mol L<sup>-1</sup> concentration in DMSO): 5.6  $\Omega^{-1}$  cm<sup>2</sup> mol<sup>-1</sup>.

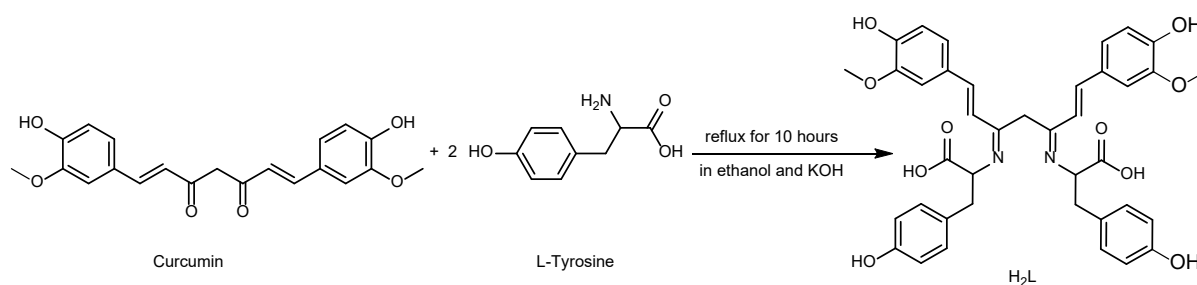
### Preparation of the [Al(L)(phen)]Cl complex

1.0 mmol aluminium(III) chloride is dissolved in 10 mL of absolute ethanol to obtain a homogeneous metal

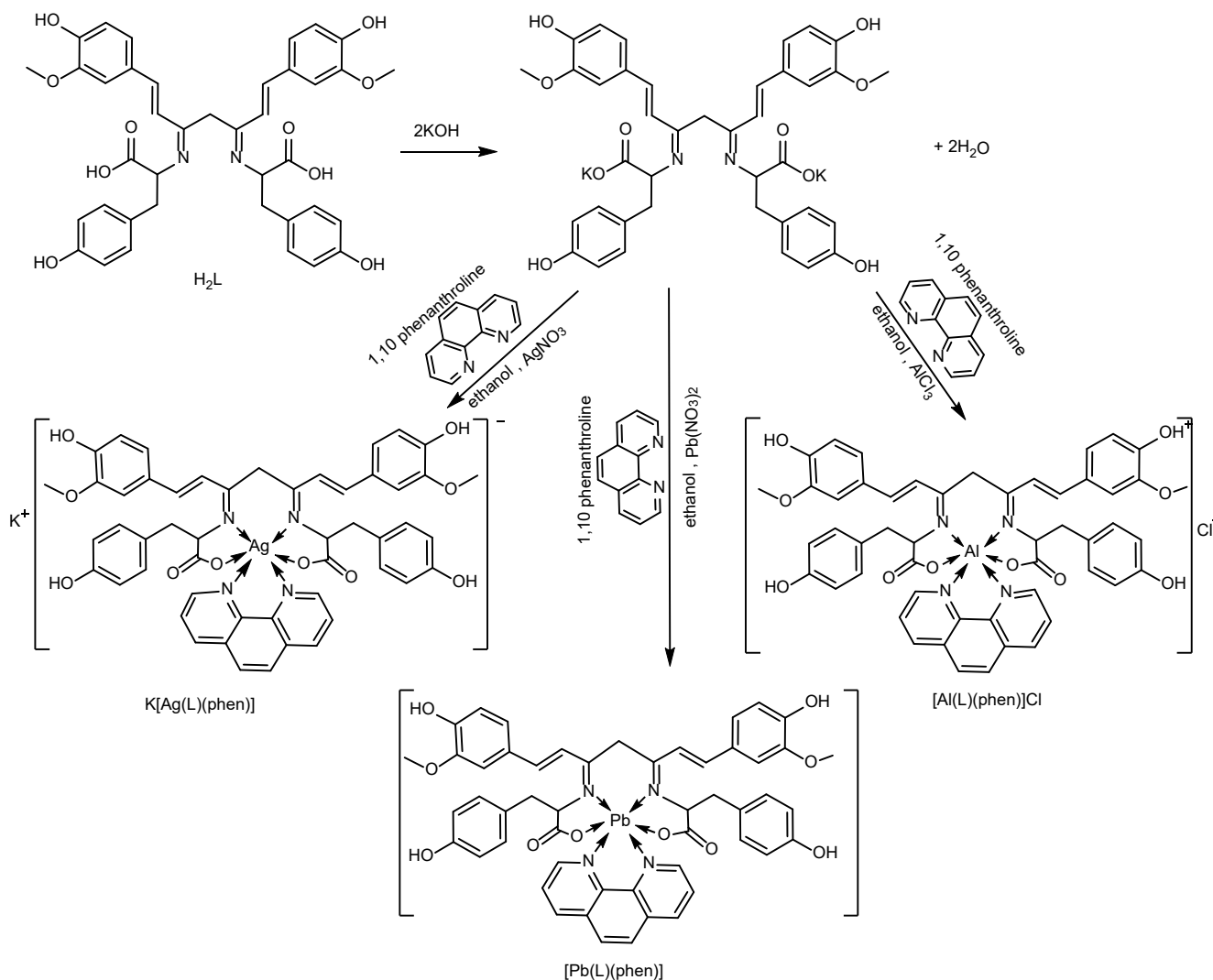
ion (Al<sup>3+</sup>) solution. A ligand solution is obtained by dissolving 1.0 mmol of Schiff base ligand, 2.0 mmol of potassium hydroxide, and 1.0 mmol of 1,10-phenanthroline in 15 mL of absolute ethanol. The ligand solution is gradually added to the metal ion (Al<sup>3+</sup>) solution with constant stirring for 30 min to obtain the precipitate. The precipitate is filtrated and washed several times in a mixture of solvent (ethanol: distilled water, 50%). The precipitate is recrystallized from the hot ethanol. The preparation of the [Al(L)(phen)]Cl complex is summarized in Scheme 2. The yield of the [Al(L)(phen)]Cl complex, was 60% (solid, Color: pale yellow, m.p. 222–224 °C). FTIR (KBr, cm<sup>-1</sup>): 3398 ( $\nu$ (O–H), phenolic), 1612 ( $\nu$ (C=N)), 1589 ( $\nu_{as}$ (COO), –COOH), 1363 ( $\nu_s$ (COO), –COOH), 1244 ( $\nu$ (C–O), phenolic), 576 ( $\nu$ (Al–O)), 474 ( $\nu$ (Al–N)). UV-Vis spectroscopy (10<sup>-3</sup> mol L<sup>-1</sup> concentration in DMSO,  $\lambda_{max}$  nm): 279, 442, 802. Metal percent in [Al(L)(phen)]Cl complex, calculated: 2.88%. Found: 3.4%. Molar conductivity (10<sup>-3</sup> mol L<sup>-1</sup> concentration in DMSO): 42.5  $\Omega^{-1}$  cm<sup>2</sup> mol<sup>-1</sup>.

### Preparation of the K[Ag(L)(phen)] complex

1.0 mmol silver(I) nitrate is dissolved in 10 mL of absolute ethanol to obtain a homogeneous metal ion (Ag<sup>+</sup>) solution. A ligand solution is obtained by dissolving 1.0 mmol of Schiff base ligand, 2.0 mmol of potassium hydroxide, and 1.0 mmol of 1,10-phenanthroline in 15 mL of absolute ethanol. The ligand solution is gradually added to the metal ion (Ag<sup>+</sup>) solution with constant stirring for 30 min to obtain the precipitate. The precipitate is filtrated and washed several times in a mixture of solvent (ethanol: distilled water, 50%). The precipitate is recrystallized from the hot ethanol. The preparation of the K[Ag(L)(phen)] complex



Scheme 1. Preparation of the Schiff base ligand



**Scheme 2.** Preparation of the  $[\text{Pb}(\text{L})(\text{phen})]$ ,  $[\text{Al}(\text{L})(\text{phen})]\text{Cl}$  and  $\text{K}[\text{Ag}(\text{L})(\text{phen})]$  complexes

is summarized in Scheme 2. The yield of the  $\text{K}[\text{Ag}(\text{L})(\text{phen})]$  complex, was 79% (solid, Color: pale brown, m.p. 188–189 °C). FTIR (KBr,  $\text{cm}^{-1}$ ): 3396 ( $\nu(\text{O}-\text{H})$ , phenolic), 1620 ( $\nu(\text{C}=\text{N})$ ), 1583 ( $\nu_{\text{as}}(\text{COO})$ ,  $-\text{COOH}$ ), 1382 ( $\nu_{\text{s}}(\text{COO})$ ,  $-\text{COOH}$ ), 1244 ( $\nu(\text{C}-\text{O})$ , phenolic), 578 ( $\nu(\text{Ag}-\text{O})$ ), 474 ( $\nu(\text{Ag}-\text{N})$ ). UV-Vis spectroscopy ( $10^{-3}$  mol  $\text{L}^{-1}$  concentration in DMSO,  $\lambda_{\text{max}}$  nm): 286, 428, 707, 829. Metal percent in  $[\text{Al}(\text{L})(\text{phen})]\text{Cl}$  complex, calculated: 10.58%. Found: 7.92%. Molar conductivity ( $10^{-3}$  mol  $\text{L}^{-1}$  concentration in DMSO): 37.2  $\Omega^{-1} \text{ cm}^2 \text{ mol}^{-1}$ .

### Computational details

Gaussian 09 software [9] is used to perform the DFT calculations. All structures of the synthesized compounds were optimized at the B3LYP/LANL2DZ level of theory

[10]. Several researchers used the LANL2DZ as a basis set in DFT calculations of systems that included Ag and Pb atoms [11-12]. The GaussView 5.0, supported by Gaussian Inc. [9], was used to generate the input files that correspond to the DFT calculations. The GaussView 5.0 software is used to visualize and analyze the data obtained from Gaussian09 output results. A frequency calculation was performed to identify the most stable structures of the synthesized compounds. The absence of the imaginary frequencies in the calculated vibrational modes indicates that the corresponding optimized structure of the molecule is the most stable one. The obtained values of the vibrational modes from the DFT calculations were scaled by a factor of 0.966 [13]. The

DFT/GIAO (gauge-independent atomic orbital) method was used to calculate and assign the  $^1\text{H}$  and  $^{13}\text{C}$ -NMR chemical shifts for carbon and hydrogen atoms of the  $\text{H}_2\text{L}$  ligand. The isotropic atomic chemical shifts in ppm unit were calculated as differences between the atomic isotropic shielding of the  $\text{H}_2\text{L}$  ligand and the corresponding reference atoms in TMS (tetramethylsilane). The energies and electron densities of the frontiers' molecular orbitals were calculated using the B3LYP level of theory and the LANL2DZ as a basis set. The excited states were computed for all compounds at the same level of theory using the TD-DFT (Time-Dependent Density Functional Theory) method [14]. The TD-DFT calculations were performed in DMSO solvent using the CPCM solvation model (conductor-like polarizable continuum model) [15]. The Projected density of states (PDOS) has been obtained through the calculated orbital populations for all compounds at the same level of theory, using GAUSSSUM 3.0 program [16].

## ■ RESULTS AND DISCUSSION

Generally, this study included synthesis Schiff base ligand ( $\text{H}_2\text{L}$ ) multi-dentate ( $\text{N}_2\text{O}_2$ ) couple negative charge derived from (1 mmol) curcumin and (2 mmol) of L-Tyrosine amino acid. The synthesized Schiff base metal complexes and some physicochemical properties are listed in Table 1.  $\text{Cl}^-$  ions were not detected by the addition of  $\text{AgNO}_3$  solution to the solutions of the three complexes for  $\text{K}[\text{Ag}(\text{L})(\text{phen})]$  and  $[\text{Pb}(\text{L})(\text{phen})]$  but

detected for  $[\text{Al}(\text{L})(\text{phen})]\text{Cl}$  complex. The  $\text{K}[\text{Ag}(\text{L})(\text{phen})]$ ,  $[\text{Pb}(\text{L})(\text{phen})]$  and  $[\text{Al}(\text{L})(\text{phen})]\text{Cl}$  complexes are stable in the air environment and have higher melting points. The solubility test indicates that these complexes are soluble in DMF, DMSO, and concentrated HCl acid. They are insoluble in  $\text{H}_2\text{O}$  and partially soluble in ethanol, acetone methanol, and most organic solvents. The molar conductivity values for  $10^{-3}$  mol  $\text{L}^{-1}$  concentration of the  $\text{K}[\text{Ag}(\text{L})(\text{phen})]$ ,  $[\text{Pb}(\text{L})(\text{phen})]$  and  $[\text{Al}(\text{L})(\text{phen})]\text{Cl}$  complexes in DMSO solvent are listed in Table 1. For the  $\text{K}[\text{Ag}(\text{L})(\text{phen})]$  and  $[\text{Al}(\text{L})(\text{Phen})]\text{Cl}$  complexes the molar conductivity are 37.2 and  $42.5 \Omega^{-1} \text{ cm}^2 \text{ mol}^{-1}$ , respectively. These results suggest that these complexes are electrolytes. The molar conductivity of the  $[\text{Pb}(\text{L})(\text{phen})]$  complex is  $5.6 \Omega^{-1} \text{ cm}^2 \text{ mol}^{-1}$ , which is revealing a non-electrolyte nature of this complex.

### Mass Spectrum

The mass spectral fragmentation of the Schiff base ligand ( $\text{H}_2\text{L}$ ) is displayed in Fig. 1. In the spectrum (Fig. 1), the peak positions of the structure consist with the formulas  $[\text{C}_{39}\text{H}_{38}\text{N}_2\text{O}_{10}]$ ,  $[\text{C}_{39}\text{H}_{36}\text{N}_2\text{O}_{10}]$ ,  $[\text{C}_{39}\text{H}_{37}\text{N}_2\text{O}_9]$ ,  $[\text{C}_{39}\text{H}_{52}\text{N}_2\text{O}_7]$ ,  $[\text{C}_{37}\text{H}_{58}\text{N}_2\text{O}_3]$  and  $[\text{C}_{36}\text{H}_{68}\text{N}_2\text{O}_2]$  appears at  $m/z$  values of 694, 692, 676, 660, 579 and 555, respectively. These spectral fragmentations allowed us to determine the molecular weight of the  $\text{H}_2\text{L}$  ligand, which is consists of the chemical formula  $[\text{C}_{39}\text{H}_{38}\text{N}_2\text{O}_{10}]$ , and equal to  $694 \text{ g mol}^{-1}$ .

**Table 1.** Formula weight, melting point, color, metal percent, percentage yield and conductivity measurement of the  $\text{H}_2\text{L}$ , phen,  $\text{K}[\text{Ag}(\text{L})(\text{phen})]$ ,  $[\text{Pb}(\text{L})(\text{phen})]$  and  $[\text{Al}(\text{L})(\text{phen})]\text{Cl}$  compounds

Compound	Formula weight ( $\text{g mol}^{-1}$ )	Color	Melting point ( $^{\circ}\text{C}$ )	Metal %	$\Lambda_m$ ( $\Omega^{-1} \text{ cm}^2 \text{ mol}^{-1}$ )	% Yield
$\text{H}_2\text{L}$	694.25	Yellow brown	150–152	-	-	81
phen	180.21	-	-	-	-	-
$[\text{Al}(\text{L})(\text{phen})]\text{Cl}$	935.36	Pale yellow	222–224	2.88 <sup>a</sup> 3.4 <sup>b</sup>	37.2 <sup>c</sup>	60
$\text{K}[\text{Ag}(\text{L})(\text{phen})]$	1019.90	Pale brown	188–189	10.58 <sup>a</sup> 7.92 <sup>b</sup>	42.5 <sup>c</sup>	79
$[\text{Pb}(\text{L})(\text{phen})]$	1080.13	Brown	156–158	19.18 <sup>a</sup> 18.01 <sup>b</sup>	5.6 <sup>c</sup>	89

<sup>a</sup>: theoretical value calculated from the molecular formula of the complex, <sup>b</sup>: experimental value where determined according to the reported method in reference [17], <sup>c</sup>: measured in DMSO

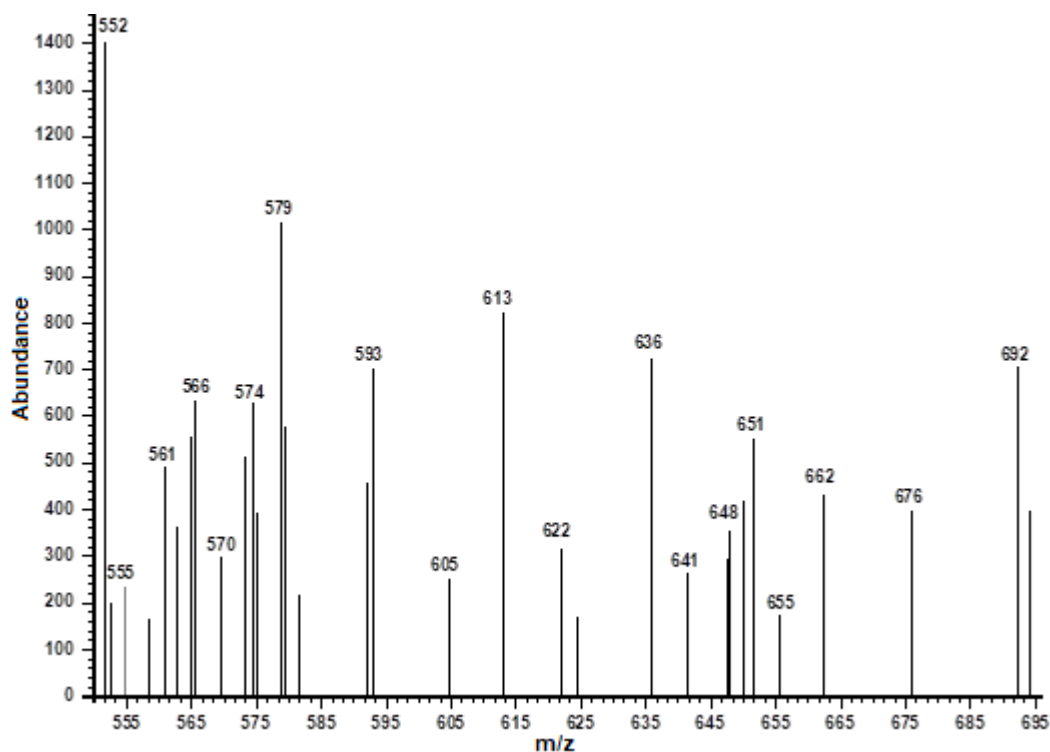


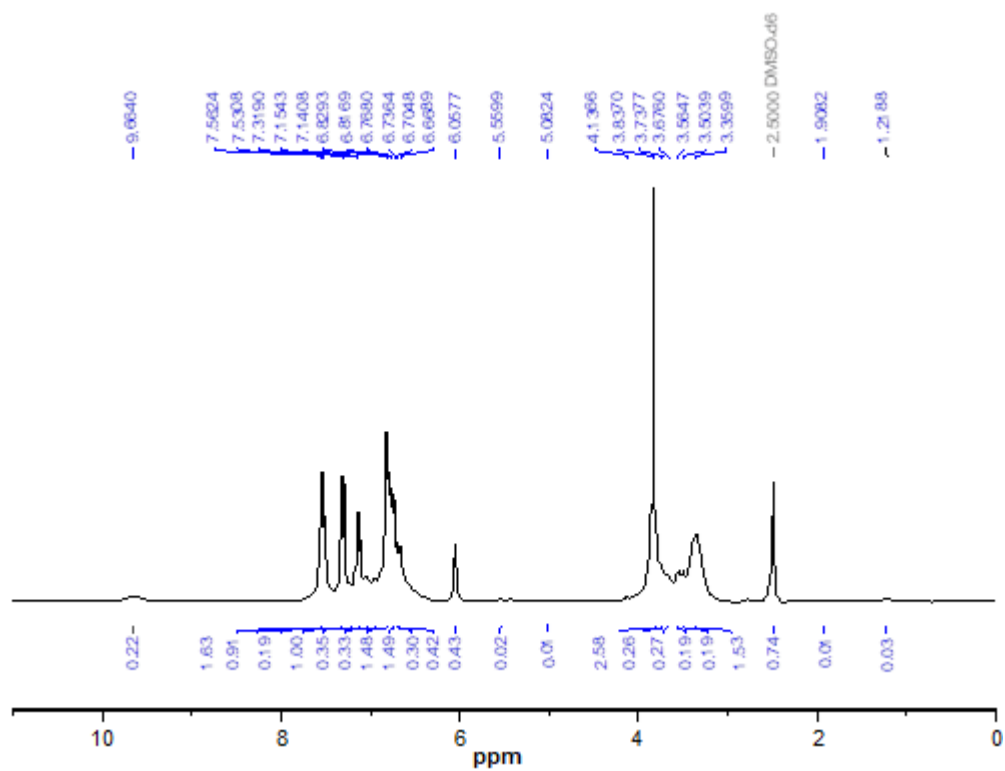
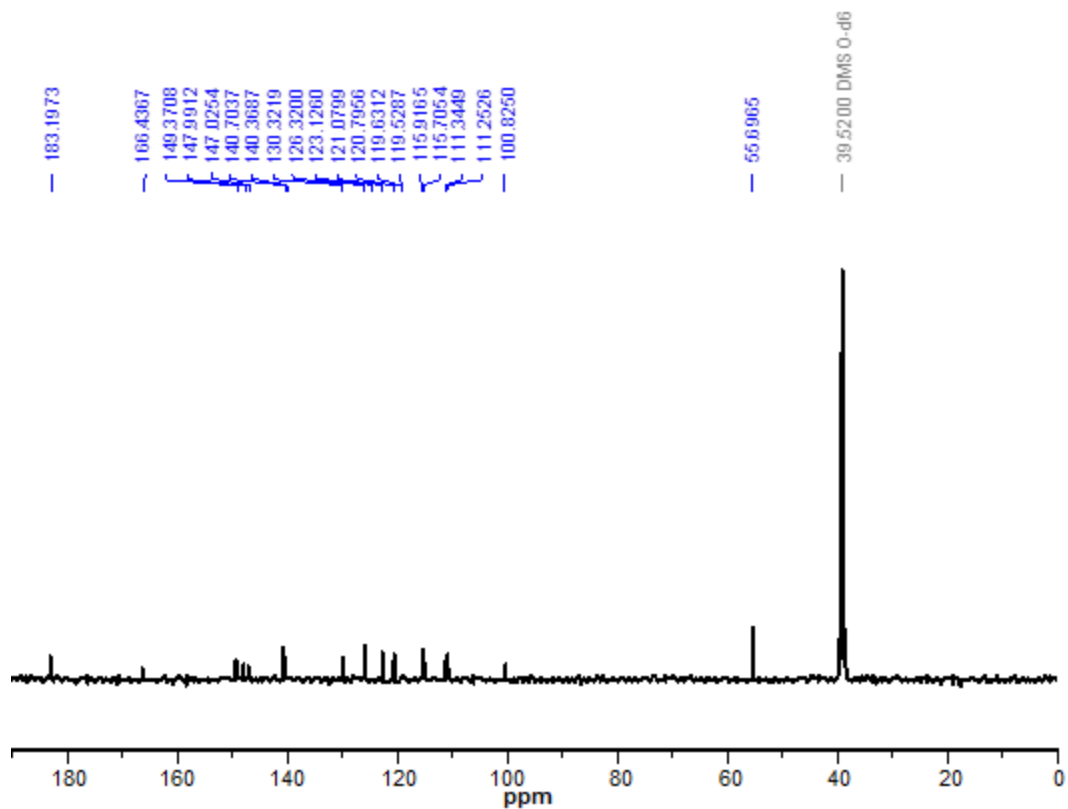
Fig 1. Fragmentation mass spectrum of Schiff base ( $H_2L$ )

### $^1H$ and $^{13}C$ -NMR Spectra of the Tetradentate Schiff Base Ligand ( $H_2L$ )

$^1H$ -NMR spectrum of the prepared Schiff base ligand,  $H_2L$ , in DMSO solvent is shown in Fig. 2. In Fig. 2, a signal appeared at 9.66 ppm which corresponds to the hydrogen atom of the phenolic hydroxyl group. According to the DFT/GIAO calculations, the theoretical chemical shift value of the proton of the phenolic hydroxyl group is obtained at 9.44 ppm. Multiples peaks appear in the range of 6.83–6.66 ppm and 7.56–7.32 ppm are corresponding to the benzene ring protons [18]. The calculated values for these peaks are in perfect agreement with those obtained experimentally, and they are observed in the range of 7.77–7.21 and 6.90–6.35 ppm. The peaks at 6.06 and 7.15 ppm are assigned to the protons of the  $C=CH$  group. The calculated chemical shift value of the  $C=CH$  group protons are at 5.74 and 7.10 ppm. The peak at 3.83 ppm is assigned to the protons of the  $OCH_3$  [19–20]. The calculated chemical shift value, obtained by the DFT/GIAO method, of the  $OCH_3$  protons, appeared at 3.80 ppm. The multiples peaks that appeared in the range 3.74–3.36 ppm correspond to the

CH and  $CH_2$  groups. The corresponding calculated chemical shift values of the proton of the CH and  $CH_2$  groups are in the range of 3.41–3.00 ppm. The missing of the carboxylic proton signal in the spectrum of Fig. 2 is due to hydrogen bonding in the ligand structure [21].

The  $^{13}C$ -NMR spectrum of tetradentate Schiff base ligand ( $H_2L$ ) is shown in Fig. 3. The spectrum of Fig. 3 shows a clear a strong peak at 183.2 ppm, which is an attribute to the carbonyl moiety of the carboxylic group [22]. The calculated chemical shift value of the carbon atom of the carboxylic group appears at 178.6 ppm. Also, peaks appeared at 149.4, 166.4, 148.0–147.0, 140.7–140.4, and 130.3 ppm are assigned to the carbons of the  $C-OH$  (carbon of benzene ring),  $C=N$  (azomethine),  $C-OCH_3$  (carbon of benzene ring),  $C=C$  (ethylene) and  $(HOOC-C-H-N)$  groups, respectively [23]. The calculated peaks corresponding to the chemical shift of the carbons of the  $C-OH$  (carbon of benzene ring),  $C=N$  (azomethine),  $C-OCH_3$  (carbon of benzene ring),  $C=C$  (ethylene), and  $(HOOC-C-H-N)$  groups are observed at 149.7, 163.8, 146.0–145.2, 143.7–143.0, and 136.4 ppm, respectively. In the recorded spectrum, the peaks correspond to the

Fig 2.  $^1\text{H}$ -NMR spectrum of tetradentate Schiff base ( $\text{H}_2\text{L}$ )Fig 3.  $^{13}\text{C}$ -NMR spectrum of tetradentate Schiff base ( $\text{H}_2\text{L}$ )

aromatic ring that appears in the range 111.3–126.3 ppm [24] and in the calculated one appears in the range 109.0–135.0 ppm. Additional signals appear at 55.7 ppm and are assigned to the methoxy carbons [25]. The calculated chemical shift value of the carbon atom of the methoxy carbon of the H<sub>2</sub>L is very close to each other and appears at 56.75 ppm and 56.59 ppm. The chemical shift value of the carbon of the methylene (CH<sub>2</sub>) group is observed at 100.8 ppm experimentally. The calculated chemical shift value of the carbon atom of the methylene group is 106.3 ppm.

### Vibrational Frequencies Results

Selected vibrational frequencies of infrared spectra of the [Al(L)(phen)]Cl, K[Ag(L)(phen)], and [Pb(L)(phen)] complexes and the H<sub>2</sub>L ligand are given in Table 2. The assignments for the observed infrared bands were based on the calculated vibrational modes and the literature data [26–30]. The spectrum of the H<sub>2</sub>L ligand shows a band at 3508, 3400, 1629, 1595, and 1425 cm<sup>-1</sup> which are attributed to  $\nu(\text{O-H})_{\text{carboxylic}}$ ,  $\nu(\text{O-H})_{\text{phenolic}}$ ,  $\nu(\text{C=N})_{\text{azomethine}}$ ,  $\nu_{\text{as}}(\text{COO})$  and  $\nu_{\text{s}}(\text{COO})$ , respectively. The  $\nu(\text{O-H})_{\text{carboxylic}}$  band disappeared in the infrared spectra of all complexes. This result confirms a complete replacement of the H<sup>+</sup> of the carboxylic group of the H<sub>2</sub>L ligand by K<sup>+</sup> during the synthesis steps of the complexes (Scheme 1). The  $\nu(\text{C=N})_{\text{azomethine}}$ ,  $\nu_{\text{as}}(\text{COO})$ , and  $\nu_{\text{s}}(\text{COO})$  bands appear at lower vibrational frequencies in the infrared spectra of all complexes as compared to those of the H<sub>2</sub>L ligand. The shifting to the lower frequencies of

these bands indicates coordination via the oxygen atom of the carboxylic group and nitrogen of the azomethine group of the H<sub>2</sub>L ligand with the metal ion. The phenolic  $\nu(\text{C-O})$  band appears in the infrared spectra of all complexes at wavenumbers very close to that of the H<sub>2</sub>L ligand (Table 2). This result indicates that the phenolic hydroxyl group of the H<sub>2</sub>L ligand did not participate in the coordination with the metal ions. In the infrared spectra of all complexes, new bands at 464–474 cm<sup>-1</sup> and 576–578 cm<sup>-1</sup> are observed and attributed to the  $\nu(\text{M-N})$  and  $\nu(\text{M-O})$ , respectively. The appearance of these bands supported the coordination of the H<sub>2</sub>L ligand with the metal ions via oxygen and nitrogen atoms.

### UV-Vis Spectra

The UV-vis spectra of the prepared ligand and its complex were recorded using 10<sup>-3</sup> M concentration of each compound in DMSO solvent. The results of the UV-visible measurements of these compounds are listed in Table 3. The UV-vis spectrum of the ligand L shows only two peaks. The first absorption peak appears at 272 nm (36765 cm<sup>-1</sup>) and is assigned to  $\pi \rightarrow \pi^*$ . This transition corresponds to the aromatic ring and double bonds fragments of the ligand L. The second absorption peak appears at 433 nm (23095 cm<sup>-1</sup>) and is assigned to  $n \rightarrow \pi^*$  transition. This transition corresponds to the azomethine ( $-\text{C}=\text{NH}$ ), hydroxyl, amine, and methoxy groups of the ligand L. This conclusion is based on that these groups are possessing non-shared electronic pairs [31]. The UV-visible spectra of the K[Ag(L)(phen)],

**Table 2.** Infrared absorption (in cm<sup>-1</sup>) data as observed and calculated for the H<sub>2</sub>L, K[Ag(L)(phen)], [Pb(L)(phen)] and [Al(L)(phen)]Cl compounds

Compound	$\nu(\text{O-H})_{\text{carboxylic}}$	$\nu(\text{O-H})_{\text{phenolic}}$	$\nu(\text{C=N})$	$\nu_{\text{as}}(\text{COO})$	$\nu_{\text{s}}(\text{COO})$	$\nu(\text{C-O})_{\text{phenolic}}$	$\nu(\text{M-O})$	$\nu(\text{M-N})$
H <sub>2</sub> L	3508 (3579) <sup>a</sup>	3400 (3526) <sup>a</sup>	1629 (1622) <sup>a</sup>	1595 (1597) <sup>a</sup>	1425 (1445) <sup>a</sup>	1244 (1249) <sup>a</sup>	-	-
[Al(L)(phen)]Cl	-	3398 (3574) <sup>a</sup>	1612 (1601) <sup>a</sup>	1589 (1590) <sup>a</sup>	1363 (1366) <sup>a</sup>	1244 (1243) <sup>a</sup>	576 (583) <sup>a</sup>	474 (478) <sup>a</sup>
k[Ag(L)(phen)]	-	3396 (3527) <sup>a</sup>	1620 (1629) <sup>a</sup>	1583 (1580) <sup>a</sup>	1382 (1390) <sup>a</sup>	1244 (1242) <sup>a</sup>	578 (576) <sup>a</sup>	474 (480) <sup>a</sup>
[Pb(L)(phen)]	-	3435 (3592) <sup>a</sup>	1620 (1634) <sup>a</sup>	1581 (1582) <sup>a</sup>	1384 (1380) <sup>a</sup>	1246 (1244) <sup>a</sup>	576 (573) <sup>a</sup>	464 (456) <sup>a</sup>

<sup>a</sup>: Calculated value according to B3LYP/LANL2DZ level,  $\nu_{\text{s}}$ : symmetric stretching;  $\nu_{\text{as}}$ : asymmetric stretching;  $\nu$ : stretching; M: the corresponding metal

**Table 3.** Computed excitation energies, electronic transition configurations, and oscillator strengths ( $f$ ) for the optical transitions in the visible region of the L ligand and the complexes (transitions with  $f \geq 0.01$  are listed)

Compound	Experimental results		TD-DFT results	
	$\lambda_{\max}$ (nm)	$\lambda_{\max}$ (nm)	Oscillator strength ( $f$ )	Major contributions
$H_2L$	272	289	0.4171	$H_{-3} \rightarrow L, H_{-2} \rightarrow L, H_{-2} \rightarrow L_{+1}, H_{-1} \rightarrow L$
		282	0.1513	$H_{-3} \rightarrow L, H_{-2} \rightarrow L_{+1}, H_{-1} \rightarrow L_{+1}$
	433	427	0.4254	$H_{-1} \rightarrow L, H \rightarrow L_{+1}$
		425	0.2227	$H_{-3} \rightarrow L, H_{-1} \rightarrow L, H \rightarrow L_{+1}$
[Al(L)(phen)]Cl	279	290	0.0706	$H \rightarrow L_{+2}$
	442	427	0.2941	$H_{-2} \rightarrow L, H \rightarrow L$
		423	0.0624	$H_{-3} \rightarrow L_{+1}, H_{-3} \rightarrow L_{+2}, H_{-1} \rightarrow L$
	802	795	0.0803	$H_{-2} \rightarrow L, H \rightarrow L$
K[Ag(L)(phen)]	268	261	0.0444	$H_{-1} \rightarrow L_{+1}, H \rightarrow L_{+1}$
	428	411	0.0217	$H_{-1} \rightarrow L, H \rightarrow L$
	707	720	0.0251	$H_{-3} \rightarrow L, H_{-2} \rightarrow L, H \rightarrow L$
	829	335	0.0163	$H_{-3} \rightarrow L, H \rightarrow L, H \rightarrow L_{+1}, H \rightarrow L_{+2}$
[Pb(L)(phen)]	271	295	0.0144	$H_{-6} \rightarrow L, H \rightarrow L_{+2}$
	435	418	0.0122	$H_{-4} \rightarrow L, H_{-2} \rightarrow L, H \rightarrow L_{+1}$
		730	0.116	$H_{-3} \rightarrow L, H_{-1} \rightarrow L$
	735	728	0.0137	$H \rightarrow L$

H: HOMO, L: LUMO

[Al(L)(phen)] Cl, and [Pb(L)(phen)] complexes show appearing of peaks at different frequency values from that of the ligand  $H_2L$ . Also, the UV-visible spectra of the complexes show the appearance of new frequencies that corresponds to charge transfer. These results support the coordination of the ligand L with metal ions.

In the UV-visible spectrum of [Al(L)(phen)]Cl complex three peaks appeared. The first peak appeared at 279 nm ( $358842 \text{ cm}^{-1}$ ) with high intensity and corresponded to intra ligand transition. The second peak is due to the charge transfer and appears at 442 nm ( $22624 \text{ cm}^{-1}$ ). The third peak appears at 802 nm ( $12469 \text{ cm}^{-1}$ ). This peak is attributed to metal (Al)  $\rightarrow$  ligand (L) transition. The Al $\rightarrow$ L transition was detected by monitoring  $4s \rightarrow 3p$  emission from Al(4s) atoms produced by pre disengagement of the excited complex [32].

The UV-visible spectrum of K[Ag(L)(phen)] complex shows the appearance of four peaks at 268 nm ( $37313 \text{ cm}^{-1}$ ), 428 nm ( $23364 \text{ cm}^{-1}$ ), 707 nm ( $14144 \text{ cm}^{-1}$ ) and 829 nm ( $12063 \text{ cm}^{-1}$ ). The peaks at 268 nm ( $37313 \text{ cm}^{-1}$ ) and 428 nm ( $23364 \text{ cm}^{-1}$ ) correspond to  $\pi \rightarrow \pi^*$  and  $n \rightarrow \pi^*$  transitions, respectively. The other two peaks are assigned to ligand-metal charge transfer transitions [23].

The UV-visible spectrum of [Pb(L)(phen)] complex shows a three peaks at 271 nm ( $36900 \text{ cm}^{-1}$ ), 435 nm ( $22989 \text{ cm}^{-1}$ ) and 735 nm ( $13605 \text{ cm}^{-1}$ ). The transitions at 271 nm ( $36900 \text{ cm}^{-1}$ ) and 435 nm ( $22988 \text{ cm}^{-1}$ ) correspond to conjugated  $\pi$  system and they are due to  $\pi \rightarrow \pi^*$  and to  $n \rightarrow \pi^*$  transitions, respectively. The third peak appeared at the visible area and corresponds to L-M charge transfer (C.T) transitions from COO $^-$  groups [32-33]. The three complexes are also diamagnetic as expected from their electron configuration [18]. The electronic spectral studies confirm the octahedral geometry of these complexes [33]. Furthermore, the complexes K[Ag(L)(phen)], [Al(L)(phen)]Cl and [Pb(L)(phen)] are diamagnetic as indicated from its magnetic moment measurements. These results support the conclusion drawn from the electronic spectral data of these complexes. The experimental data, which are obtained from the electronic spectra and the magnetic measurements values of the complexes, are in good agreement with the calculated optimized structure of these.

#### DFT Calculations and Electronic Structures

The optimized structures of the K[Ag(L)(phen)],

[Al(L)(phen)]Cl, and [Pb(L)(phen)] complexes according to the B3LYP/LANL2DZ level of theory are displayed in Fig. 4. Selected bond distances and bond angles of the optimized structures of these complexes are listed in Table 4. The observations from the calculated geometries that displayed in Fig. 4 show that the environment surrounding the central metal ion in [Al(L)(phen)]Cl, K[(Ag(L)(phen))] and [Pb(L)(phen)] complexes adopted distorted octahedral configuration. The distorted octahedral of the environment surrounding the central metal atom of these complexes is due to the tension that comes from the formation of three rings around the central metal upon complexation.

The calculated bond length of Ag(1)-N(45), Ag(1)-N(46), Ag(1)-N(2) and Ag(1)-N(3) of the K[Ag(L)(phen)] complex (Table 4) are 2.534, 2.663, 2.590 and 2.383 Å, respectively. The typical Ag-N bond lengths are reported within the range 2.1–2.7 Å [34–37]. Moreover, the calculated Ag-N bond lengths of the

K[Ag(L)(phen)] complex is shorter than the sum of the van der Waals radii of N and Ag atoms (1.55 and 1.72 Å, respectively) [38]. The calculated bond length of Ag(1)-O(5) and Ag(1)-O(4) of the K[Ag(L)(phen)] complex (Table 4) are 2.685 and 2.291 Å, respectively. These values are within the reported Ag-O bond lengths range (2.032–2.754 Å) [35,39–40]. It should be noted that the calculated Ag-O bond lengths are not larger than the sum of the van der Waals radii of O and Ag atoms, which are 1.52 and 1.72 Å, respectively [38].

The optimized geometry of the [Al(L)(phen)]K complex (Fig. 4, Table 4), shows that the bond length of Al(86)-N(45), Al(86)-N(44), Al(86)-N(2), Al(86)-N(1), Al(86)-O(4) and Al(86)-O(3) are 2.173, 2.104, 2.035, 2.072, 1.852 and 1.862 Å, respectively. Previous studies concerning the complexation of Al<sup>3+</sup> with Schiff base reported that the bond lengths of Al-N and Al-O are within the range of 1.988–2.013 Å and 1.809–1.881 Å, respectively [41–42]. The values of Al-N and Al-O bond

**Table 4.** Selected bond lengths (Å) and bond angles (°) of the computed structures of the [Al(L)(phen)]Cl, K[(Ag(L)(phen))] and [Pb(L)(phen)] according to B3LYP/LANL2DZ level of theory

Bond Lengths (Å) of [Al(L)(phen)]Cl		Bond Lengths (Å) of K[(Ag(L)(phen))]		Bond Lengths (Å) of [Pb(L)(phen)]	
N(45)-Al(86)	2.173	Ag(1)-N(45)	2.534	N(45)-Pb(86)	2.839
N(44)-Al(86)	2.104	Ag(1)-N(46)	2.663	N(44)-Pb(86)	2.834
O(4)-Al(86)	1.852	Ag(1)-O(5)	2.685	O(4)-Pb(86)	2.212
O(3)-Al(86)	1.869	Ag(1)-O(4)	2.291	O(3)-Pb(86)	2.198
N(2)-Al(86)	2.035	Ag(1)-N(2)	2.590	N(2)-Pb(86)	2.805
N(1)-Al(86)	2.072	Ag(1)-N(3)	2.383	N(1)-Pb(86)	2.876
Angles (°) of [Al(L)(phen)]Cl		Angles (°) of K[(Ag(L)(phen))]		Angles (°) of [Pb(L)(phen)]	
N(45)-Al(86)-N(44)	76.971	N(45)-Ag(1)-N(46)	64.660	N(45)-Pb(86)-N(44)	58.427
N(45)-Al(86)-O(4)	87.035	N(45)-Ag(1)-O(5)	125.009	N(45)-Pb(86)-O(4)	72.281
N(45)-Al(86)-O(3)	162.718	N(45)-Ag(1)-O(4)	77.569	N(45)-Pb(86)-O(3)	120.065
N(45)-Al(86)-N(2)	91.706	N(45)-Ag(1)-N(2)	104.920	N(45)-Pb(86)-N(2)	119.812
N(45)-Al(86)-N(1)	96.998	N(45)-Ag(1)-N(3)	140.505	N(45)-Pb(86)-N(1)	170.595
N(44)-Al(86)-O(4)	93.885	N(46)-Ag(1)-O(5)	71.337	N(44)-Pb(86)-O(4)	113.284
N(44)-Al(86)-O(3)	86.462	N(46)-Ag(1)-O(4)	140.734	N(44)-Pb(86)-O(3)	74.989
N(44)-Al(86)-N(2)	168.384	N(46)-Ag(1)-N(2)	134.896	N(44)-Pb(86)-N(2)	178.054
N(44)-Al(86)-N(1)	97.718	N(46)-Ag(1)-N(3)	93.132	N(44)-Pb(86)-N(1)	117.487
O(4)-Al(86)-O(3)	99.112	O(5)-Ag(1)-O(4)	128.663	O(4)-Pb(86)-O(3)	97.193
O(4)-Al(86)-N(2)	82.802	O(5)-Ag(1)-N(2)	129.654	O(4)-Pb(86)-N(2)	64.938
O(4)-Al(86)-N(1)	168.303	O(5)-Ag(1)-N(3)	70.209	O(4)-Pb(86)-N(1)	116.531
O(3)-Al(86)-N(2)	105.033	O(4)-Ag(1)-N(2)	63.609	O(3)-Pb(86)-N(2)	105.833
O(3)-Al(86)-N(1)	80.200	O(4)-Ag(1)-N(3)	124.233	O(3)-Pb(86)-N(1)	63.777
N(2)-Al(86)-N(1)	86.098	N(2)-Ag(1)-N(3)	66.915	N(2)-Pb(86)-N(1)	64.387

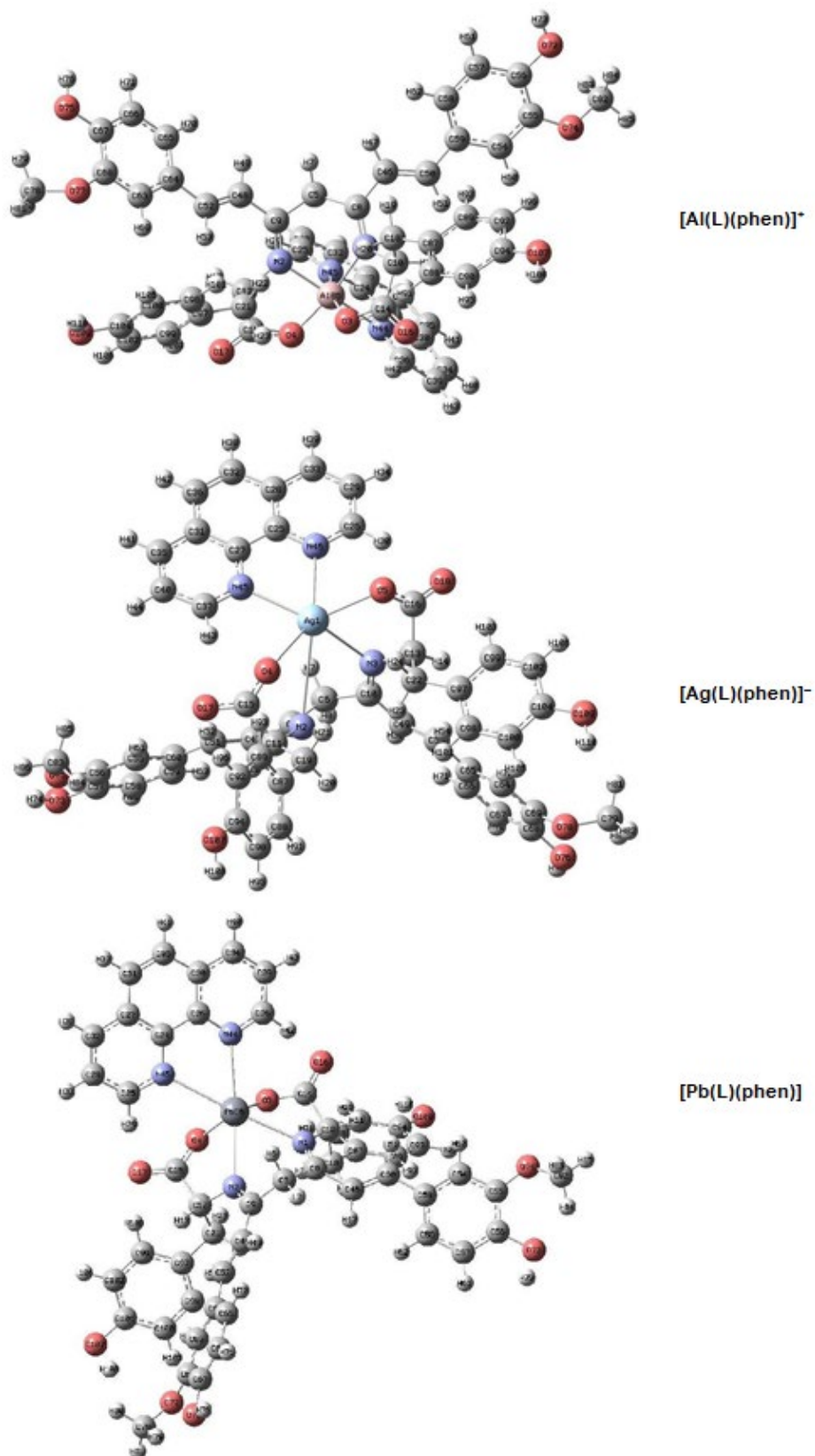


**Fig 4.** Optimized structures of [Al(L)(phen)]<sup>+</sup>, [Ag(L)(phen)]<sup>-</sup> and [Pb(L)(phen)] complexes according to B3LYP/LANL2DZ level of theory

lengths reported in these studies are very close to those obtained in our study.

The bond lengths of Pb(86)–N(45), Pb(86)–N(44), Pb(86)–N(2), Pb(86)–N(1), Pb(86)–O(4) and Pb(86)–O(3) that presented by the optimized structure of the [Pb(L)(phen)] complex (Fig. 4, Table 4) are 2.839, 2.834, 2.805, 2.876, 2.212 and 2.198 Å, respectively. These bond lengths are in the range of the Pb–N and Pb–O bond lengths reported in the literature [43-45].

The UV-Vis measurements of the synthesized H<sub>2</sub>L ligand and complexes were performed in DMSO solvent. All these compounds show several absorption bands in the UV-Vis region (Table 3). TD-DFT (Time-Dependent Density Functional Theory) calculations were performed on the optimized geometries of the synthesized complexes and H<sub>2</sub>L ligand to assign these bands. The calculated absorption spectra of the compounds, which are obtained from the output of the TD-DFT computations, were simulated using the GaussSum software. The simulated and experimental UV-Vis spectra of the synthesized H<sub>2</sub>L ligand and complexes are in good agreement (Table 3). To demonstrate the electronic properties of the synthesized

complexes, investigations were performed on the calculated energies and electron densities of the frontiers molecular orbitals. Fig. 5 summarizes the energy profile of the highest occupied molecular orbitals (HOMO's) and lowest unoccupied molecular orbital (LUMO's), and HOMO-LUMO gaps for [Ag(L)(phen)]<sup>-</sup>, [Al(L)(phen)]<sup>+</sup> and [Pb(L)(phen)] complexes, which are calculated at the B3LYP/LANL2DZ level of theory. The higher HOMO-LUMO energy gap is associated with the [Pb(L)(phen)] complex. The orbital energies and percent composition of selected frontier occupied and virtual molecular orbitals of complexes, expressed in terms of composing fragments, calculated at the B3LYP/LANL2DZ level are listed in Table 5. As shown in Table 5, the metal of the [Al(L)(phen)]<sup>+</sup> complex is contributing only 1% to the LUMO, and LUMO<sub>+1</sub> orbitals. The presented frontier occupied orbitals of the [Al(L)(phen)]<sup>+</sup> complex in Table 5 are completely localized on the L ligand, while the virtual orbitals are mostly localized on the phen ligand. The HOMO and LUMO contour plots of [Al(L)(phen)]<sup>+</sup> complex are shown in Fig. 6.

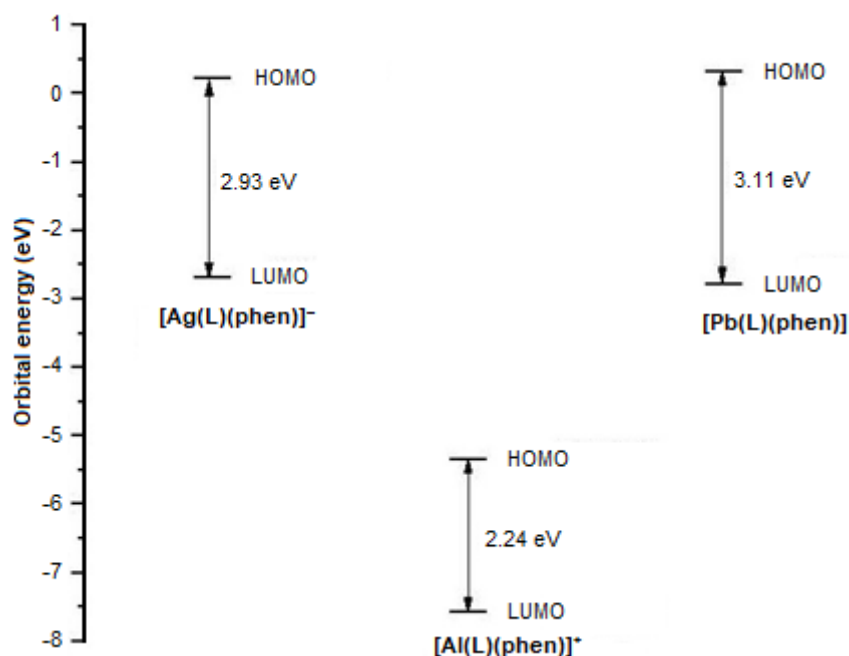


**Fig 5.** Energy profile of the highest occupied molecular orbitals (HOMO's) and lowest unoccupied molecular orbital (LUMO's), and HOMO-LUMO gaps for [Ag(L)(phen)]<sup>-</sup>, [Al(L)(phen)]<sup>+</sup> and [Pb(L)(phen)] complexes, calculated at the B3LYP/ LANL2DZ level of theory

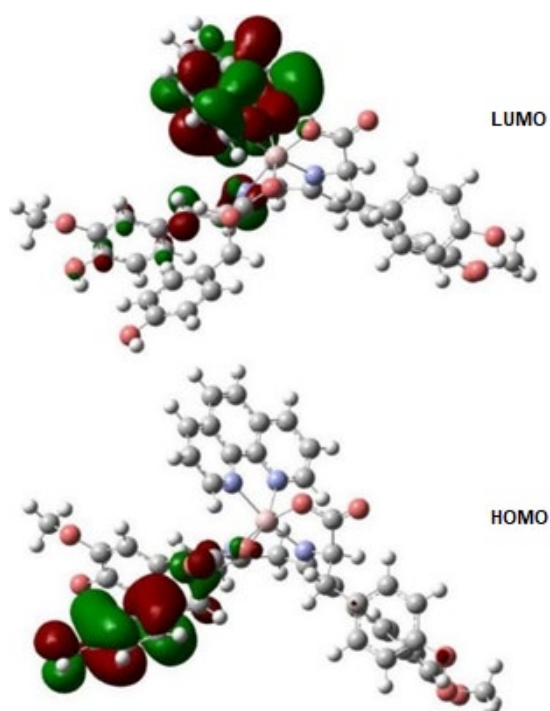


**Fig 6.** The frontier orbitals HOMO and LUMO of  $[\text{Al}(\text{L})(\text{phen})]^+$  calculated at the B3LYP/LANL2DZ level of theory, with the surface isovalue is 0.02

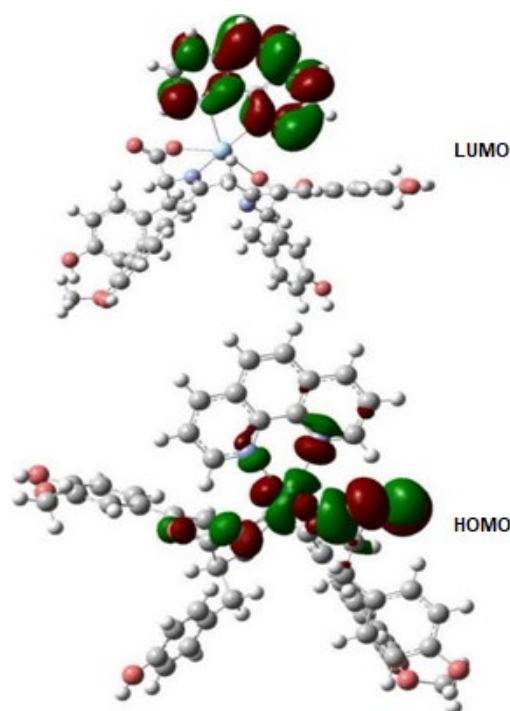


**Fig 7.** The frontier orbitals HOMO and LUMO of  $[\text{Ag}(\text{L})(\text{phen})]^-$  calculated at the B3LYP/LANL2DZ level of theory, with the surface isovalue is 0.02

The percent composition of the frontier molecular orbitals of  $[\text{Ag}(\text{L})(\text{phen})]^-$  complex are different from that of  $[\text{Al}(\text{L})(\text{phen})]^-$  as shown in Table 5. The metal of the  $[\text{Ag}(\text{L})(\text{phen})]^-$  complex is a notable contribution to the HOMO, HOMO<sub>-1</sub>, and HOMO<sub>-2</sub> orbitals with the percentage of 25, 18, and 18%, respectively. The presented frontier occupied orbitals of the  $[\text{Ag}(\text{L})(\text{phen})]^-$  complex is mostly localized on the L ligand. Concerning the virtual orbitals, LUMO and LUMO<sub>+2</sub>, are localized with the percentage of 100 and 99%, respectively on the phen ligand. The virtual orbital, LUMO<sub>+1</sub>, is localized with a percentage of 99% on the L ligand. The HOMO and LUMO contour plots of  $[\text{Ag}(\text{L})(\text{phen})]^-$  complex is shown in Fig. 7.

The presented frontier orbitals, LUMO<sub>+1</sub>, LUMO, HOMO, HOMO<sub>-1</sub>, HOMO<sub>-2</sub>, HOMO<sub>-3</sub>, HOMO<sub>-4</sub>, HOMO<sub>-5</sub>, and HOMO<sub>-6</sub> of the  $[\text{Pb}(\text{L})(\text{phen})]$  complex are localized on the L ligand with the percentage of 100, 99, 94, 90, 98, 84, 85, 93 and 98%, respectively. The LUMO<sub>+2</sub> orbital is completely localized on phen ligand. The metal of the  $[\text{Pb}(\text{L})(\text{phen})]$  complex is contributed only to the HOMO<sub>-1</sub>, HOMO<sub>-2</sub>, HOMO<sub>-3</sub>, HOMO<sub>-4</sub>, HOMO<sub>-5</sub>, and

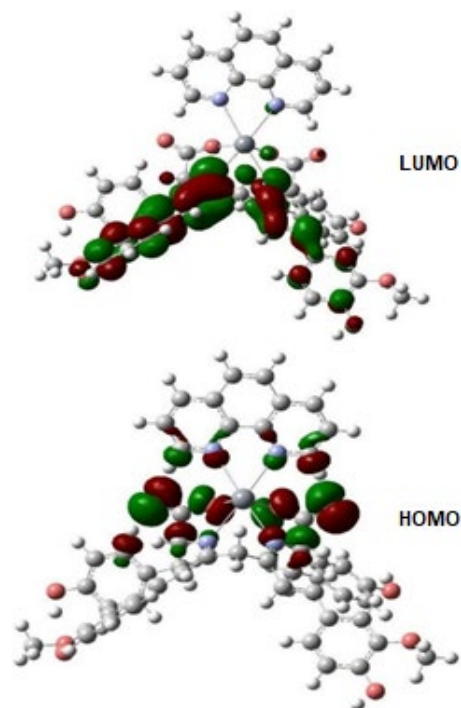


**Fig 8.** The frontier orbitals HOMO and LUMO of  $[\text{Pb}(\text{L})(\text{phen})]$  calculated at the B3LYP/LANL2DZ level of theory, with the surface isovalue is 0.02

**Table 5.** Percent composition in terms of composing fragments of selected frontier molecular orbitals (MO's) and molecular orbitals energies of the complexes calculated at the B3LYP/LANL2DZ level

Complexes	MO	MO energy (eV)	Fragment		
			Metal	phen ligand	L ligand
[Al(L)(phen)]Cl	L <sub>+2</sub>	-5.00	0	82	17
	L <sub>+1</sub>	-5.23	1	26	73
	L	-5.34	1	89	10
	H	-7.58	0	0	100
	H <sub>-1</sub>	-7.65	0	0	100
	H <sub>-2</sub>	-8.16	0	0	100
	H <sub>-3</sub>	-8.30	0	0	100
K[Ag(L)(phen)]	L <sub>+2</sub>	0.31	1	99	0
	L <sub>+1</sub>	0.28	0	1	99
	L	0.23	0	100	0
	H	-2.70	25	6	69
	H <sub>-1</sub>	-2.79	18	5	77
	H <sub>-2</sub>	-3.01	18	2	80
	H <sub>-3</sub>	-3.19	5	3	92
[Pb(L)(phen)]	L <sub>+2</sub>	0.76	0	100	0
	L <sub>+1</sub>	0.53	0	0	100
	L	0.32	0	1	99
	H	-2.79	0	6	94
	H <sub>-1</sub>	-2.92	5	5	90
	H <sub>-2</sub>	-3.04	1	1	98
	H <sub>-3</sub>	-3.14	13	3	84
	H <sub>-4</sub>	-3.38	5	10	85
H <sub>-5</sub>	-3.43	2	4	93	
H <sub>-6</sub>	-3.51	1	1	98	

H: HOMO, L: LUMO

HOMO<sub>-6</sub> orbitals. The HOMO and LUMO contour plots of [Pb(L)(phen)] complex are shown in Fig. 8.

## ■ CONCLUSION

The Schiff base ligand (H<sub>2</sub>L) has been prepared from curcumin and L- Tyrosine amino acid. The synthesized Schiff base ligand (H<sub>2</sub>L) and the second ligand 1,10-phenanthroline (phen) are used to prepare the new mixed ligand complexes [Al(L)(phen)]Cl, K[Ag(L)(phen)] and [Pb(L)(phen)]. The results obtained from the UV-visible spectra and the magnetic moments values of the complexes are in good agreement with the optimized structures of these compounds, which are calculated according to B3LYP/LANL2DZ level of the theory. The optimized structures of [Al(L)(phen)]Cl, K[Ag(L)(phen)]

and [Pb(L)(phen)] that calculated according to B3LYP/LANL2DZ level of the theory show that the environment surrounding the central metal ion in these complexes adopted distorted octahedral configuration. The computed energies and electron densities of the frontiers molecular orbitals were reported. All these results indicate that experimental and theoretical calculations were consistent.

## ■ AUTHOR CONTRIBUTIONS

The authors Ali Mahmood Ali and Tagreed Hashim Al-Noor conducted the synthesise and measurement experiments, and the authors Eid Abdalrazaq, and Abdel Aziz Qasem Jbarah conducted the DFT calculations, wrote and revised the manuscript. All authors agreed to

the final version of this manuscript.

## ■ REFERENCES

- [1] Omidi, S., and Kakanejadifard, A., 2020, A review on biological activities of Schiff base, hydrazone, and oxime derivatives of curcumin, *RSC Adv.*, 10 (50), 30186–30202.
- [2] Mahal, A., Wu, P., Jiang, Z.H., and Wei, X., 2019, Schiff bases of tetrahydrocurcumin as potential anticancer agents, *ChemistrySelect*, 4 (1), 2019, 366–369.
- [3] Kareem, A., Khan, M.S., Nami, S.A.A., Bhat, S.A., Mirza, A.U., and Nishat, N., 2018, Curcumin derived Schiff base ligand and their transition metal complexes: Synthesis, spectral characterization, catalytic potential and biological activity, *J. Mol. Struct.*, 1167, 261–273.
- [4] Priyadharshini, N., Iyyam, P.S., Subramanian, S., and Venkatesh, P., 2015, Synthesis, spectroscopic characterization and DNA interaction of Schiff base curcumin Cu(II), Ni(II) and Zn(II) complexes, *Der Pharma Chem.*, 7 (10), 186–201.
- [5] Ferenc, W., Osypiuk, D., Sarzyński, J., and Gluchowska, H., 2020, Complexes of Mn(II), Co(II), Ni(II), Cu(II) and Zn(II) with ligand formed by condensation reaction of isatin with glutamic acid, *Eclética Quím. J.*, 45, 12–27.
- [6] Bhanuka, S., and Singh, H.L., 2016, Synthesis, spectroscopic and molecular studies of lead(II) complexes of Schiff bases derived from 4-methoxybenzaldehyde and amino acids, *Rasāyan J. Chem.*, 9 (4), 614–626.
- [7] Shukla, S., and Mishra, A.P., 2013, Synthesis, structure, and anticancerous properties of silver complexes, *J. Chem.*, 2013, 527123.
- [8] Pradhan, A., and Kumar, A., 2015, A review: An overview on synthesis of some Schiff bases and their metal complexes with antimicrobial activity, *Chem. Process Eng. Res.*, 35, 84–86.
- [9] Frisch, M.J., Trucks, G.W., Schlegel, H.B., Scuseria, G.E., Robb, M.A., Cheeseman, J.R., Scalmani, G., Barone, V., Mennucci, B., Petersson, G.A., Nakatsuji, H., Caricato, M., Li, X., Hratchian, H.P., Izmaylov, A.F., Bloino, J., Zheng, G., Sonnenberg, J.L., Hada, M., Ehara, M., Toyota, K., Fukuda, R., Hasegawa, J., Ishida, M., Nakajima, T., Honda, Y., Kitao, O., Nakai, H., Vreven, T., Montgomery Jr., J.A., Peralta, J.E., Ogliaro, F., Bearpark, M., Heyd, J.J., Brothers, E., Kudin, K.N., Staroverov, V.N., Keith, T., Kobayashi, R., Normand, J., Raghavachari, K., Rendell, A., Burant, J.C., Iyengar, S.S., Tomasi, J., Cossi, M., Rega, N., Millam, J.M., Klene, M., Knox, J.E., Cross, J.B., Bakken, V., Adamo, C., Jaramillo, J., Gomperts, R., Stratmann, R.E., Yazyev, O., Austin, A.J., Cammi, R., Pomelli, C., Ochterski, J.W., Martin, R.L., Morokuma, K., Zakrzewski, V.G., Voth, G.A., Salvador, M.P., Dannenberg, J.J., Dapprich, S., Daniels, A.D., Farkas, O., Foresman, J.B., Ortiz, J.V., Cioslowski, J., and Fox, D.J., 2009, *Gaussian 09, Revision D.01*, Gaussian, Inc., Wallingford CT.
- [10] Al-Razaq, E.A., Buttrus, N., Al-Kattan, W., Jbarah, A.A., and Almatarneh, M., 2011, Reactions of Pd<sup>2+</sup> and Pt<sup>2+</sup> with pyrrolidinedithio carbamate and cystine ligands: Synthesis and DFT calculations, *J. Sulfur Chem.*, 32 (2), 159–169.
- [11] Thanakit, P., Suramit, S., and Phromyothin, D., 2017, The study of metal binding properties and electronic transitions of dithienopyrrole derivatives, *Mater. Today: Proc.*, 4 (5), 6585–6591.
- [12] Chen, X., Hu, Y., Gao, J., Zhang, Y., and Li, S., 2013, Interaction of melamine molecules with silver nanoparticles explored by surface-enhanced Raman scattering and density functional theory calculations, *Appl. Spectrosc.*, 67 (5), 491–497.
- [13] Assefa, M.K., Devera, J.L., Brathwaite, A.D., Mosley, J.D., and Duncan M.A., 2015, Vibrational scaling factors for transition metal carbonyls, *Chem. Phys. Lett.*, 640, 175–179.
- [14] Cossi, M., and Barone, V., 2001, Time-dependent density functional theory for molecules in liquid solutions, *J. Chem. Phys.*, 115 (10), 4708–4717.
- [15] Cossi, M., Rega, N., Scalmani, G., and Barone V., 2003, Energies, structures, and electronic properties of molecules in solution with the C-PCM solvation model, *J. Comput. Chem.*, 24 (6), 669–681.

- [16] O'Boyle, N.M., Tenderholt, A.L., and Langner, K.M., 2008, cclib: A library for package-independent computational chemistry algorithms, *J. Comput. Chem.*, 29 (5), 839–845.
- [17] Ali, H.R.H., Saleh, G.A., Hussein, S.A., and Hassan, A.I., 2013, Preparation, characterization and atomic absorption spectroscopic determination of some metal complexes of glipizide, *Der Pharma Chem.*, 5 (6), 156–163.
- [18] Shahraki, S., and Delarami, H.S., 2018, Magnetic chitosan-(D-glucosimine methyl)benzaldehyde Schiff base for Pb<sup>+2</sup> ion removal. Experimental and theoretical methods, *Carbohydr. Polym.*, 200, 211–220.
- [19] Shah, A.D., Raval, D.J., Jatakiya, V.P., Sen, D.J., and Badmanaban, R., 2012, Comparison study of antimicrobial activity with effect of DPPH for antioxidant study of synthesized Schiff bases of Mannich bases of resacetophenone having variable electronegative atoms, *Int. J. Drug Dev. Res.*, 4 (2), 205–215.
- [20] Yousif, E., Majeed, A., Al-Sammarrae, K., Salih, N., Salimon, J., and Abdullah, B., 2017, Metal complexes of Schiff base: Preparation, characterization and antibacterial activity, *Arabian J. Chem.*, 10 (Suppl. 2), S1639–S1644.
- [21] Dehkhodaei, M., Khorshidifard, M., Rudbari, H.A., Sahihi, M., Azimi, G., Habibi, N., Taheri, S., Bruno, G., and Azadbakht, R., 2017, Synthesis, characterization, crystal structure and DNA, HSA-binding studies of four Schiff base complexes derived from salicylaldehyde and isopropylamine, *Inorg. Chim. Acta*, 466, 48–60.
- [22] Gandhi, S.R., Kumar, D.S., Tajudeen, S.S., and Sheriff, A.K.I., 2017, Studies on synthetic, structural characterization, thermal, DNA cleavage, antimicrobial and catalytic activity of tetradentate (N<sub>4</sub>) Schiff base and its transition metal complexes, *Asian J. Chem.*, 29, 1076–1084.
- [23] Singh, H.L., and Singh, J.B., 2012, Synthesis and characterization of new lead(II) and organotin(IV) complexes of Schiff bases derived from histidine and methionine, *Int. J. Inorg. Chem.*, 2012, 568797.
- [24] Balić, T., Marković, B., and Medvidović-Kosanović, M., 2015, Electrochemical and structural analysis of a novel symmetrical bis-Schiff base with herringbone packing motif, *J. Mol. Struct.*, 1084, 82–88.
- [25] de Lima, D.P., Giannesi, G.C., dos Santos, E.A., Freitas, T.S.E., Lopes, R.S., Lopo, M.N., Beatriz, A., Marques, M.R., and Marchetti, C.R., 2017, N-acetylation of aromatic amines by the soil fungus *Aspergillus japonicus* (UFMS 48.136), *Lett. Org. Chem.*, 14 (4), 227–230.
- [26] Abdel-Rahman, L.H., Ismail, N.M., Ismael, M., Abu-Dief, A.M., and Ahmed, E.A.H., 2017, Synthesis, characterization, DFT calculations and biological studies of Mn(II), Fe(II), Co(II) and Cd(II) complexes based on a tetradentate ONNO donor Schiff base ligand, *J. Mol. Struct.*, 1134, 851–862.
- [27] Keypour, H., Aidi, M., Mahmoudabadi, M., Karamian, R., Asadbegy, M., and Gable, R.W., 2019, Synthesis, X-ray crystal structural, antioxidant and antibacterial studies of new Cu(II) macrocyclic Schiff base complex with a ligand containing homopiperazine moiety, *J. Mol. Struct.*, 1198, 126666.
- [28] Singh, H.L., and Singh, J., 2014, Synthesis, spectroscopic, molecular structure, and antibacterial studies of dibutyltin(IV) Schiff base complexes derived from phenylalanine, isoleucine, and glycine, *Bioinorg. Chem. Appl.*, 2014, 716578.
- [29] Hemalatha, S., Dharmaraja, J., Shobana, S., Subbaraj, P., Esakkidurai, T., and Raman, N., 2020, Chemical and pharmacological aspects of novel hetero MLB complexes derived from NO<sub>2</sub> type Schiff base and N<sub>2</sub> type 1,10-phenanthroline ligands, *J. Saudi Chem. Soc.*, 24 (1), 61–80.
- [30] Nakamoto, K., 2006, "Infrared and Raman spectra of inorganic and coordination compounds" in *Handbook of Vibrational Spectroscopy*, Eds. Chalmers, J.M., and Griffiths, P.R., John Wiley & Sons, Inc., Hoboken, New Jersey, US.
- [31] Savithri, K., Kumar, B.C.V., Vivek, H.K., and Revanasiddappa, H.D., 2018, Synthesis and characterization of cobalt(III) and copper(II)

- complexes of 2-((E)-(6-fluorobenzo[d]thiazol-2-ylimino)methyl)-4-chlorophenol: DNA binding and nuclease studies—SOD and antimicrobial activities, *Int. J. Spectrosc.*, 2018, 8759372.
- [32] Cotton, F.A., Wilkinson, G., Murillo, C.A., and Bochmann, M., 1999, *Advanced Inorganic Chemistry*, 6<sup>th</sup> Ed., John Wiley & Sons, Ltd., Chichester, UK.
- [33] Lever, A.B.P., 1984, *Inorganic Electronic Spectroscopy*, Series: Studies in Physical and Theoretical Chemistry, Vol. 33, Elsevier, Amsterdam.
- [34] Gulbransen, J.L., and Fitchett, C.M., 2012, Anion directed control of supramolecular structure in silver complexes through weak interactions, *CrystEngComm*, 14 (7), 5394–5397.
- [35] Pettinari, C., Marchetti, F., Orbisaglia, S., Pettinari, R., Ngoune, J., Gómez, M., Santos, C., and Álvarez, E., 2013, Group 11 complexes with the bidentate di(1*H*-indazol-1-yl)methane and di(2*H*-indazol-2-yl)methane ligands, *CrystEngComm*, 15 (19), 3892–3907.
- [36] Nunes, J.H.B., de Paiva, R.E.F., Cuin, A., Lustrì, W.R., and Corbi, P.P., 2015, Silver complexes with sulfathiazole and sulfamethoxazole: Synthesis, spectroscopic characterization, crystal structure and antibacterial assays, *Polyhedron*, 85, 437–444.
- [37] Kim, Y., and Kang, S.K., 2015, Crystal structure of bis-[2-(1*H*-benzimidazol-2-yl)aniline]silver(I) nitrate, *Acta Crystallogr., Sect. E: Crystallogr. Commun.*, 71 (Pt 9), 1058–1060.
- [38] Bondi A., 1964, van der Waals volumes and radii, *J. Phys. Chem.*, 68 (3), 441–451.
- [39] Soliman, S.M., Mabkhot, Y.N., Barakat, A., and Ghabbour, H.A., 2017, A highly distorted hexacoordinated silver(I) complex: synthesis, crystal structure, and DFT studies, *J. Coord. Chem.*, 70 (8), 1339–1356.
- [40] Bergamini, F.R.G., Ferreira, M.A., de Paiva, R.E.F., Gomes, A.F., Gozzo, F.C., Formiga, A.L.B., Corbi, F.C.A., Mazali, I.O., Alves, D.A., Lancellotti, M., and Corbi, P.P., 2012, A binuclear silver complex with L-buthionine sulfoximine: Synthesis, spectroscopic characterization, DFT studies and antibacterial assays, *RSC Adv.*, 2 (27), 10372–10379.
- [41] Asadi, Z., Asadi, M., and Shorkaei, M.R., 2016, Synthesis, characterization and DFT study of new water-soluble aluminum(III), gallium(III) and indium(III) Schiff base complexes: Effect of metal on the binding propensity with bovine serum albumin in water, *J. Iran. Chem. Soc.*, 13 (3), 429–442.
- [42] Truscott, J.C., Conradie, J., Swart, H.C., Duvenhage, M.M., and Visser, H.G., 2019, Synthesis, crystal structures, photoluminescence, electrochemistry and DFT study of aluminium(III) and gallium(III) complexes containing a novel tetra-dentate Schiff base ligand, *Acta Crystallogr., Sect. C: Cryst. Struct. Commun.*, 75 (8), 1045–1052.
- [43] Ghanbari, B., and Zarepour-Jevinani, M., 2016, Synthesis and characterization of M(II) (M = Cd, Hg and Pb) complexes with naphthodiaza-crown macrocyclic ligand and study of metal ion recognition by fluorescence, <sup>1</sup>H NMR spectroscopy, and DFT calculation, *J. Coord. Chem.*, 69 (18), 2793–2803.
- [44] Platas-Iglesias, C., Esteban-Gómez, D., Enríquez-Pérez, T., Avecilla, F., de Blas, A., and Rodríguez-Blas, T., 2005, Lead(II) thiocyanate complexes with bibracchial lariat ethers: An X-ray and DFT study, *Inorg. Chem.*, 44 (7), 2224–2233.
- [45] Mahmoudi, G., Seth, S.K., Riera, A.B., Zubkov, F.I., and Frontera, A., 2020, Novel Pb(II) complexes: X-ray structures, Hirshfeld surface analysis and DFT calculations, *Crystals*, 10 (7), 568.